Influence of natural fibers characteristics on the interface mechanics with cement based matrices

Saulo Rocha Ferreira
Departamento de Engenharia, Universidade Federal de Lavras, Brazil
Email: saulo.ferreira@deg.ufla.br
Civil Engineering Department, COPPE, Universidade Federal do Rio de Janeiro,
21941-972 RJ, Brazil
e-mail: ferreira.sr@coc.ufrj.br

Marco Pepe
Department of Civil Engineering, University of Salerno, via Giovanni Paolo II 132, 84084,
Fisciano (SA), Italy.
e-mail: mapepe@unisa.it

Enzo Martinelli,
Department of Civil Engineering, University of Salerno, via Giovanni Paolo II 132, 84084,
Fisciano (SA), Italy.
e-mail: e.martinelli@unisa.it

Flávio de Andrade Silva
Civil Engineering Department, Pontifícia Universidade Católica do Rio de Janeiro (PUC-Rio), 22451-900 RJ, Brazil
email: fsilva@puc-rio.br

Romildo Dias Toledo Filho
Civil Engineering Department, COPPE, Universidade Federal do Rio de Janeiro,
21941-972 RJ, Brazil
e-mail: toledo@coc.ufrj.br
Corresponding author: toledo@coc.ufrj.br

The final version of this manuscript is available in *Composites Part B: Engineering*. 10.1016/j.compositesb.2017.12.016

ABSTRACT

The use of Natural Fibers in cementitious composites is an innovative technical solution but, they are characterized by a complex microstructure and significant heterogeneity, which influence their interaction with cementitious matrices, whose identification requires further advances in the current state of knowledge. The present study summarizes the results of a wide series of pull-out tests carried out on sisal, curaua and jute fibers. Then, the experimental results are employed in an inverse identification procedure aimed at unveiling the key features of the aforementioned bond-slip laws. Morphological, chemical, physical and mechanical characterization of the natural fibers were correlated with the resulting bond properties within the embedding matrix. The obtained results in terms of relevant parameters, such as bond strength and fracture energy (under pull-out stresses) of the fiber-matrix interface, pave the way for future studies intended for a better understanding of the structural response of Natural Fiber Reinforced Cementitious Composites.

KEYWORDS: A. Fibres, B. Fibre/matrix bond, C. Analytical modelling, D. Mechanical testing.

1. INTRODUCTION

The use of fibers as a dispersed reinforcement in cement-based materials is a common solution for enhancing post-cracking response of cementitious matrices in a class of materials generally referred to as Fiber-Reinforced Cementitious Composites (FRCCs) [1]. In fact, FRCCs are generally characterized by higher tensile and flexural strength, tougher and more ductile post-cracking behavior and superior durability performance [2], as fibers promote a "bridging effect" across the opening cracks and lead to enhanced response in the post-peak branch of stress-strain relationships [3]. This effect is controlled by several relevant parameters, such as fiber geometry [4], shape [5], dosage [6], orientation and distribution within the matrix, mechanical properties of fibers and bond interaction between fiber and cementitious matrix [7].

On the other hand, nowadays, the construction sector is being challenged to "go green" in many aspects including to find more environmental friendly processes and innovation technologies by using biodegradable materials [8][9]. For these reasons, research activities have been recently developed for demonstrating the potential of using natural fibers [10][11], in a class of materials often referred to as Natural Fiber Reinforced Cementitious Composites (N-FRCCs) [12][13]. In fact, N-FRCCs have the potentiality to become the ultimate green construction material option, minimizing the use of natural resources and overall lifetime impact [14]. As a matter of principle, due to many advantages, it's expected that natural fiber-cement based composites will expand their usage in the near coming future. This new trend is motivated by the lower cost of these fibers with respect to the "ordinary" industrial fibers, either made of steel or plastic materials [15].

The natural fibers are derived from vegetable raw materials and are generally characterized by a complex microstructure[16][17][18] but they present excellent mechanical performance being characterized by tensile strength, generally, higher than 200 MPa [19][20]. For instance, sisal fibers are among the most promising, in fact, investigation about their morphology (in terms of transverse section area and shape) and mechanical properties have been recently developed [21]: these studies demonstrate that the relevant geometric and physical parameters of these fibers are comparable to the ones of various types of industrial fibers [21]. On the other hand, in order to promote the use of natural reinforcement for cement-based construction materials, the interface mechanism occurring between natural fibers and cement-based matrix should be more deeply investigated [22][23][24].

In this context, the present study is mainly intended at identifying the bond-slip laws capable to describe the interaction of natural fibers embedded within cementitious matrices. First, it summarizes the results of a wide series of pull-out tests carried out on sisal, curauá and jute fibers. Then, the experimental results are employed in an inverse identification procedure aimed at unveiling the key features of the aforementioned bond-slip laws [25]. Morphological, physical, chemical and mechanical characterization of the natural fibers were also performed and these results are

The final version of this manuscript is available in *Composites Part B: Engineering*. 10.1016/j.compositesb.2017.12.016

correlated with the resulting bond properties within the embedding matrix. Finally, some possible correlations between the main parameters (i.e., bond strength and fracture energy) of the aforementioned bond-slip laws and the fiber type and morphology are figured out.

It is worth highlighting that, despite the intrinsic heterogeneity that is expected to characterize natural fibers (in terms of both geometric and mechanical properties), the present study aims at identifying the parameters of a bond-slip law whose formulation has been chosen with the aim to balance accuracy and simplicity.

2. MATERIALS AND METHODS

2.1 Fibers

This study considers three types of natural fibers: sisal, curauá and jute. These fibers are characterized by lengths ranging from 40 cm to 100 cm, depending on the original source (either leaves or stalk) and extraction process.

All fibers underwent a preliminary washing treatment in hot water (80-100°C) intended at removing any existing residues, such as fats, waxes and mucilage, from their surface. Heating was performed in a still pan filled with tap water warmed up at a gradient of 1ºC/min. After reaching the required temperature, the fibers were held in water for one hour and, immediately after washing, the fibers were dried without thermal shock. Then, after drying, the fibers were brushed by means of a laboratory metallic comb with the aim to facilitate their cutting with a guillotine-like device.

Sisal fibers were obtained from homonymous plants, whose scientific name is "*Agave sisalana*": these plants are grown in farms located in the state of Bahia, Brazil. The fibers were removed from the leaves in the form of long fiber bundles through the so-called "decortication" process, in which leaves are crushed by a rotating wheel with blunt knives.

Curauá fibers were supplied by Pematec, a dealer located in the city of Santarém, in the state of Pará, Brazil. They were extracted from the leaves of "*Ananas erectifolius*", present in Amazonia, by means of a process similar to the one adopted for sisal fibers.

Finally, jute fibers also came from Amazonia. More specifically, they were extracted from the stem of the plant "*Corchorus capsularis*" by means of a process consisting of cutting, retting, shredding, drying, packing and classification [26].

2.2 The cement based matrix

The cementitious matrix of the Natural FRCC investigated in this work, was based on a binder consisting of 30% Portland cement CP-32 F II [27], 30% metakaolin and 40% fly ash (in weight). As already demonstrated in previous researches [26], this amount of metakaolin guarantees durability of fibers within the cement matrix. Moreover, the presence of fly ash mainly aims at ensuring workability: in fact, it induces a more uniform distribution of fibers within

the cementitious matrix [28]. The cementitious matrix was obtained by mixing two parts of binder for each part of sand, and adopting 0.4 as water-to-cement ratio.

The sand was processed in order to obtain a maximum diameter equal to 840 μm. In addition, a superplasticizer (Glenium 51 - type PA) with solids content of 31% was used and, 0.8 kg/m^3 of a viscosity modifier Rheomac UW 410 were also added with the aim to avoid segregation during the casting process.

2.3 Experimental procedures

2.3.1 Morphological and mechanical characterization of the natural fibers

The natural fiber's microstructure was investigated using an SEM Hitachi TM3000. The microscope was operated under an accelerating voltage of 15 kV. A working distance of 3 mm was applied and tilt was set to 0º. A pre-coating with a thin layer of approximately 20 nm of gold was done to make the fiber conductive and suitable for analysis. In order to measure the fiber's cross-sectional area, for each single fiber used in the pullout and tensile test, and adjacent piece of the fiber (immediately next to the one tested) was kept for future measurement and morphology characterization using the SEM.

More specifically, a sample was taken out of each fiber undergoing mechanical tests. The obtained images were, then, post-processed by using ImageJ, a Java-based image processing program [29]. For roughness analysis, a topography image and phase contrast was obtained using an Atomic Force Microscope (1M Plus, JPK Instruments, Germany). Images were obtained in dynamic mode using a Micromasch NSC 14/AIBS cantilever with nominal spring constant of 5 N/m. Force–distance curves were systematically obtained mapping a selected 20 μm × 20 μm region of the sample in an 8×8 points matrix. Curves were automatically analyzed for slope and adhesion of the retrace curve providing distribution maps. Force–distance curve data were obtained using the same cantilever used to image the samples in the intermittent contact mode.

The mechanical behavior of natural fibers was investigated by performing tensile tests in a Shimadzu AG-X electromechanical testing machine, equipped with a load cell of 1.0 kN. The fibers, with a gage length of 40 mm, were glued to a paper mold to get both a better alignment in the machine and a sufficient grip with the upper and lower jaws in accordance to ASTM C1557 [30]. For each type of fiber, 15 tests were performed at a displacement rate of 0.1 mm/min: the tensile strength of fibers was determined by dividing the maximum force measured in these tests by the transverse section area measured by analyzing the images obtained through SEM.

2.3.2 Physical and mechanical characterization of the matrix

Several parameters were measured for evaluating the main physical and mechanical properties of the cement matrix under investigation. Specifically, water absorption, density and void contents, were determined in accordance with ASTM C642 [31]; flow table spread value were measured according to ASTM C1437 [32]; compressive strength at 7

and 28 days was determined in accordance with ASTM C39 [33]; Static Elastic modulus and tensile strength were also determined according to ASTM C496 [34] and RILEM recommendation [35], respectively. Table 1 summarizes the results for the aforementioned measurements.

2.3.4 Single fiber pull-out tests

In order to investigate the bond interaction between fibers and matrix, pull-out tests were carried out by means an electromechanical testing machine Shimadzu AG-X with a load cell of 1.0 kN: Figure 1 depicts the equipment employed in these pullout tests, which were executed in displacement control at a rate of 0.1 mm/min. The test specimens were prepared in special molds and three different embedment lengths (namely, 5, 10 and 25 mm) were realized. The tests were performed after 6 days of curing in a fog room (100% RH) plus 1 day of drying at T=23º C ± 1ºC and relative humidity of 65% ± 3%. In fact, previous studies performed by the Authors [36] highlighted that, for the cement-based matrix used in this study, after 7 days of curing no significant increasing were registered for both matrix tensile strength as well as the its elastic modulus: As a matter of fact, these parameters govern the bond-slip behavior of the embedded fibers.

3 EXPERIMENTAL RESULTS

3.1 Morphological characterization of natural fibers

Figure 2 shows the typical microstructure of natural fibers: they present individual fiber-cells, linked together by means of the middle lamella (ML), which consist of hemicellulose and lignin. Each individual fiber-cell consists of four main parts, namely the primary wall, the thick secondary wall, the tertiary wall and the lumen. The natural fibers, generally, present similar morphology, but they differ from each other in terms of various parameters, such as the internal area of lumens, number of lumens, the number and size of fiber-cells, secondary cell-walls thickness and the real cross-section (the total area minus the lumen area). These parameters were evaluated for the natural fibers considered in this study and the main results are summarized in Table 2. Sisal fibers are constituted by about of 140 fiber cells and present the higher value of lumen area (around 5800 μm^2); on the other hand, curauá fibers present the highest number of fiber-cells (300) and the lowest lumens area (around 360 μm^2) and diameter (0.8 μm); jute fibers are constituted by the lowest amount of fiber-cells (26), characterized by a lumen area of around 1000 μm^2 (Table 2).

Figure 3 shows some examples of the cross section for the natural fibers under investigation. As expected, their transverse section is irregular in shape and non-uniform throughout the fiber length. The cross section of the sisal fiber can be categorized in three typical recurring shapes [37]: *horse-shoe* shape (characterizing fibers derived from the external area of the leaf); *arched* shape (typical for sisal fibers derived from the center of the leaf) and *twisted* shape (this shape is a consequence of the extraction process in which the arched fibers are twisted). On the other hand, curauá

fibers present a typical serrated *oval* shape, whereas jute fibers have a peculiar shape resembling a *comma* (Figure 3): this label can be attributed to the thin elongated and low curve geometry.

A more comprehensive analysis of the cross-section area variation of the natural fibers is presented in Figure 4 in terms of relative frequency distribution. Sisal fibers present the highest scattering range of values in comparison with curauá and jute. The latter have cross-section areas ranging between 0.0003 to 0.0115 mm^2, whereas sisal fibers range between 0.015 to 0.054 mm^2. The lower dispersion characterizing transverse sections in curauá and jute fibers may be attributed to the more uniform fiber shape in comparison with the sisal ones (Figure 3). As a matter of the fact, according to the results reported in Figure 4, sisal fibers area characterized by a multimodal distribution with the identification of three peaks indicate three different populations of results: the first, located between 0.015-0.030, another between 0.024-0.039 and other between 0.039 to 0.054. These variations can be correlated to the three different cross-section shapes mentioned above. Similarly, cross section perimeter was also evaluated (Figure 5): sisal, curauá and jute fibers present an average perimeter equal to 0.751 mm, 0.979 mm and 0.863 mm, respectively. Moreover, according to the results plotted in Figure 5, sisal fiber presents the highest dispersion in terms of perimeter relative frequency in comparison with the other fibers (perimeter values ranging from 0.4 to 1.2 mm): this can be a directly correlated to variability in cross section shape. It is worth highlighting that the aforementioned perimeter and area were determined as average values throughout the fiber length.

Besides the qualitative classification of fibers morphology, based on the area and perimeter measurements, a quantitative parameter, such as the relative Fiber Intrinsic Efficiency Ratio (FIER), was introduced for determining an objective measure of their shape [38]. It is defined as follows:

$$FIER = \frac{P_f}{P_{eq}} \tag{1}$$

where P_f is the actual fiber perimeter of the fiber and P_{eq} is the circumference of a cylindrical fiber characterized by the same cross sectional area measured on the natural fiber. Some examples of fibers cross-section shapes are presented in Figure 3 meanwhile the relative frequency distribution for the $FIER_r$ values is shown in Figure 6. The values of FIER obtained for the sisal, curauá and jute fibers analyzed in this study present an average of 1.3 (ranging between 1.1 and 2.0), 3.4 (ranging between 1.7 and 7.9) and 4.3 (ranging be-tween 2.5 and 6.2), respectively. This result confirms that the natural fibers under investigation are characterized by a significantly irregular cross section, whose shape is far different from an ideally circular one. Moreover, the average values of FIER obtained for the three shapes observed by Silva et al. [37] turned out to be 1.21, 1.38 and 1.76, respectively. Since the FIER value is direct correlated to a relation between fiber cross-section area and perimeter, curauá and jute fibers, despite presenting smaller areas in comparison with the sisal ones, show an irregular and rugged cross-section line, then increasing the perimeter: once the perimeter is

high, the FIER increases. As expected, the curauá and jute present higher values well distributed according the relative frequency. The result is a consequence of the lower area and higher perimeter values. Sisal fibers present a more uniform and lower scattering ranging FIER values.

In addition, the SEM images reported in Figure 7 highlight a twisting rotation of the transverse section throughout the fiber axis. As a matter of principle, this features tends to increase the bond between cement-based matrix and the embedded fiber [39]: from Figure 7 it emerges that the sisal fibers present the highest longitudinal axis rotation.

The morphological characterization of the natural fibers is, finally, completed with the analysis of the surface roughness that is realized with the combination of SEM microscopy, AFM phase contrast and 3D reconstruction (Figure 8).

The SEM images indicate that all the fibers present a serrated (saw-toothed) surface in the transversal direction, presenting a repetitive sequence of peaks and valleys (Figure 8): sisal and curauá present an average of 5 frequency of peaks and troughs, whereas jute fibers are characterized by around 16 frequency. Figure 8 shows that the sisal fibers present a surface characterized by pronounced peaks and troughs, curauá fibers present a granular surface, presenting a shallow roughness meanwhile jute fibers present a flat and the smoothest surface. For a better understanding of this shape variation, three lines of profile from AFM data were reproduced: (a) longitudinal, (b) transversal and (c) diagonal directions (see Figure 9).

Figure 9 confirms that jute presents a smoother surface than the two other fibers. Along the longitudinal direction, representing the path along which the pull out mechanism occurs, it is possible to observe that curauá and jute present a higher roughness meanwhile sisal presents a wide depression.

3.2 Mechanical behavior of natural fibers

The mechanical behavior of the sisal, curauá and jute fibers under consideration was evaluated through performing fifteen direct tensile tests [30].

The tensile strength of sisal, curauá and jute fibers is equal to 484, 632 and 250 MPa (with standard deviation 135, 138 and 89), respectively. Moreover, their elastic moduli are equal to 19.5, 38.1 and 43.9 GPa (with standard deviation of 4.5, 18.0 and 12.3), respectively. These results indicate that the mechanical response of all kinds of fibers present a relatively high scatter: this can be reasonably attributed to their intrinsically irregular morphology. Despite this, all the fibers analyzed in this study can be considered as a high-performance fibers presenting a tensile strength higher than 200 MPa and a relatively high elastic modulus.

Several authors in literature [22][40] have highlighted that the mechanical behavior of natural fibers is governed by both their microstructure morphology and chemical composition (governed by the total amount of cellulose each one characterized by a different crystallinity degree). The sisal fibers under investigation present approximately 60.5% of

cellulose, 25.7% of hemicelluloses and 12.1% of lignin; curauá fibers present a chemical composition that comprehends approximately 59% of cellulose, 23.8% of hemicelluloses and 14.7% of lignin and the jute fibers employed in this study present a chemical composition that comprehends approximately 74.4% of cellulose, 15% of hemicelluloses and 8.4% of lignin. According to the literature [21], fibers with high cellulose amount, generally, present a low deformation capacity and this is confirmed by the experimental evidences achieved in the present study.

3.3 Single fiber pull-out tests

Some examples of load-slip curves obtained in the tests mentioned in this section are plotted in Figure 10. More specifically, the results obtained from pull-out tests carried out on specimens of different bond length are represented therein.

The results of the single fiber pull-out tests performed on sisal, curauá and jute fibers highlight three types of curves derived from the performed tests:

- *type 1* (e.g., L5 for jute fiber in Figure 10) presents an almost elastic behavior (adhesive bond phase) up to the maximum force and then a decay of the force up to reach a constant value of the residual force (frictional bond phase);
- *type 2* (e.g., L25 for sisal fiber in Figure 10) can be interpreted as a sub case of the *type 1* mode, in fact, after the elastic phase another local peak (mechanical bond phase) is achieved an then the residual force is reached;
- *type 3* (e.g., L10 for jute fiber in Figure 10) features a first elastic branch (adhesive bond phase) but the maximum force is reached after a non-elastic phase (mechanical bond phase) an then the softening phase (mechanical/frictional bond) is less pronounced in comparison with the two previous cases.

Regarding the failure mechanism, all specimens with 5 mm bond length exhibited a debonding failure. Specifically, the three types of fibers achieved an almost equal peak force with apparently different post-peak behavior: curauá exhibited the most ductile response, whereas a more abrupt decay in axial force was observed in jute fibers. Similar considerations can be drawn out in terms of failure mechanisms observed for 10-mm length specimens. However, in this case a more significant difference emerged in terms of stiffness of the elastic branch, whereas the response of curauá and jute turned out to be basically overlapped. Conversely, different responses were observed for the 25-mm specimens. Particularly, 25-mm jute fibers failed in tension and, hence, as a result of bond interaction, geometric properties and axial strength, the tests demonstrated that transfer length can be considered between 10 and 25 mm.

4 IINVERSE IDENTIFICATION OF THE BOND-SLIP LAWS

4.1 Outline of the analytical model

An analytical model has been formulated for simulating the interaction between fiber and matrix in a pull-out process [41][25]. It assumes that:

- the fiber behaves in a linear elastic way;
- the matrix is supposed to be perfectly stiff;
- the interaction between fiber and matrix is based on a bond-slip law τ-s, invariant throughout the fiber length.

As for the last point, the model assumes the following bilinear bond-slip law (Figure 11):

$$\tau(s)=\begin{cases} k_{el}\cdot s & if \quad |s|\le s_{el} \\ \tau_r - k_{in}\cdot(s-s_{el}) & if \quad s_{el}<|s|\le s_u \\ 0 & if \quad |s|>s_u \end{cases} \tag{2}$$

where $k_{el}=\tau_{max}/s_{el}$ is the slip modulus of the elastic branch ending at a slip value s_{el} with a corresponding bond stress τ_{max}, τ_r is the residual bond stress, and k_{in} is the post-peak slip modulus (strictly positive), resulting in a linear variation of stresses from τ_r to τ_u, the latter being achieved for a slip s_u.

Based on the above assumptions, the full range analytical expression of the applied pull-out force F_0 can be determined, as a function of the displacement s_0 at the end of the fiber embedment, on the loaded side. Further details on both the mathematical derivation and the numerical implementation of this solution are available in a previous paper recently published by the Authors [25].

Since F_0 also depends upon the actual bond-slip law assumed for describing the interface behavior, the following conceptual relationship can be written:

$$F_0 = F_0(s_0;\boldsymbol{q}), \tag{3}$$

where $\boldsymbol{q}$ is a vector that collects the five parameters describing the interface law described in Figure 11:

$$\boldsymbol{q}=\begin{bmatrix} s_{el} & s_u & \tau_{max} & \tau_r & \tau_u \end{bmatrix}. \tag{4}$$

The aforementioned analytical model can be employed for determining the parameters describing the actual bond-slip interaction by means of an "inverse identification" procedure [25]. More specifically, the following optimization problem has to be solved:

$$\bar{\boldsymbol{q}} = \arg\min_{\boldsymbol{q}} \Delta(\boldsymbol{q}) \ . \tag{5}$$

being

$$\Delta(\boldsymbol{q})=\sum_{i=1}^{n}\left[F_0(s_{0,i};\boldsymbol{q})-F_{0,i}^{\ exp}\right]^2 \ . \tag{6}$$

The final version of this manuscript is available in *Composites Part B: Engineering*. 10.1016/j.compositesb.2017.12.016

where $s_{0,i}$ is the displacement imposed on the free end of the fiber at the i-th increment of the experimental procedure, $F_{0,i}^{exp}$ is the corresponding force and n is the number of displacement increments either in the experimental process or the current numerical analysis.

4.2 Bond-slip laws

The phenomenological description, outlined at the end of the previous section, suggests some insights into the interaction between fibers and matrix. However, since the resulting force-slip laws are clearly influenced by several geometric parameters, such as FIER and bond length, a deeper interpretation of the material-level interaction between the various tested fibers and matrices should be achieved by taking duly into account the structural behavior of the system under consideration.

More specifically, it can be assumed that the fiber behaves like a rod-like element connected to a stiff matrix by means of a longitudinally invariant bond-slip law capable to describe the fracture process in mode II that leads to debonding. In other words, the experimental results can be interpreted in the light of the model outlined in Section 4.1 and, hence, the bond-slip law, generally depicted in Figure 11, can be identified through the inverse procedure mathematically described by eqs. (3)-(6). Therefore, the inverse identification procedure was applied to all the force-slip curves obtained in experimental tests in which debonding failure was actually observed. Table 3, Table 4 and Table 5 summarize the results obtained for the three types of fibers tested in the experimental program outlined in Section 3.3: the values determined for the five free components of vector **q** described in eq. (4) are reported within the aforementioned tables for sisal, cuaruà and jute fibers, respectively. Moreover, the tables also mention the corresponding values of fracture energy (G_F), which can be easily determined from the five aforementioned parameters. For all these quantities, the corresponding average value and coefficient of variation (as a percentage, in round brackets) are highlighted.

Furthermore, Figure 12 shows the comparison between some of the experimental results and the corresponding numerical simulation carried out by assuming the values of Table 3, Table 4 and Table 5 for identifying the actual bond-slip law. Figure 12 demonstrates that the simplified law depicted in Figure 11 and the inverse identification procedure outlined in Section 4.1 are capable to achieve a significant accuracy in simulating the mechanical behavior and determining the relevant bond-slip laws, based on their global force-slip response observed on the tested specimens.

In fact, the choice of a bilinear-discontinuous bond-slip curve (Figure 11) is a reasonable trade-off between accuracy and simplicity: in some cases (e.g., L10 for Jute fibers in Figure 12) the simulations do not "exactly" match point-by-point the experimental results and, certainly, a "richer" and more general analytical "shape" of the bond-slip relationship would enhance the quality of approximation for each single specimen. Nevertheless, the natural specimen-to-specimen variability would not be reduced by "enriching" the analytical expression of the bond-slip curve, as the

experimental results themselves are widely scattered because of the natural variability of the relevant geometric and mechanical properties.

Moreover, it is worth highlighting that the five parameters collected in the vector **q** are often in the same order of magnitude for all the three fibers, as derived from tests on 5 and 10 mm. Conversely, the values of both displacement and stress parameters in vector **q** are generally lower when derived from the longest specimens: this is probably a result of the variability of the bond-slip law throughout the fiber, which is expected to be higher for longer fibers (and is actually neglected by the employed model). The intrinsic heterogeneity of natural fibers makes it hard (and unlikely) to define a "unique" function for the bond-slip law. In fact, even nominally identical specimens lead to variable bond-slip laws. This is due to the natural variability of geometric and mechanical properties, mainly of fibers, but also of the cement matrix. However, the "average" values of the obtained parameters (see Figure 13) can be considered for obtaining a reasonably approximate simulation of the pull-out process.

A more comprehensive analysis of the results can be performed by considering the results plotted in Figure 14 and Figure 15 where the relative frequency distribution for the key bond parameters (i.e., τ_{max} and G_F) are, respectively, reported. It should be highlighted that, in order to have a more indicative comparison between the different fibers considered herein, the data reported in these figures don't include the results derived from the pull-out tests with the higher embedded length (i.e., L25), both because in this case all the jute fibers failed and (as also highlighted before) by increasing the fiber length a higher variable (local) bond slip law is expected.

The τ_{max} values obtained from sisal, curauá and jute fibers range between 0.1 and 0.9 MPa (Figure 14): the peak bond stress value is, mostly, governed by the chemical interaction (adhesional bond) between the cement-based matrix and the embedded fiber and less influenced by the fiber morphology (mechanical bond). As a matter of the fact, the fairly unimodal distributions reported in Figure 14 for the three types of fibers under investigation, can be interpret with the fact that although the natural fibers present a highly variable morphology the τ_{max} is, mainly, defined by their chemical composition and their resulting compatibility with the cement hydration products. Figure 14 also highlights that both curauá and jute fibers present in more than 40% of the case a peak bond stress value ranging between 0.2 and 0.3 MPa, on the other hand, in the case of sisal fibers the highest relative frequency was observe in the range of 0.4 and 0.5 MPa. The higher values observed in the case of sisal fibers can be certainly related to the fact these kinds of fibers presented the more "complex" geometry but also with the fact that sisal fibers surfaces present the wider peaks and valleys in their surfaces: this allow the finer particles of cement and pozzolanic addition to settle in the fibers' surface and created a denser microstructure surrounding the sisal fiber. An explanation of this phenomenon is proposed in Figure 16a, in which a SEM image, performed on a sisal fiber after the pull-out test, is reported.

The same kind of analysis can be performed by considering the results in terms of fracture energy (Figure 15). Unlike the bond stress, the G_F values are governed by the fiber morphology since it plays a fundamental role on the definition of the mechanical and frictional bond. As a matter of the fact, the distributions reported in Figure 15 highlight that in most of the cases, the jute fibers present a fracture energy varying between a short range (0-0.4 N/mm). On the other hand, the curauá and jute fibers almost do not present peaks in the distribution, but a fairly uniform distribution (up to the range of 1.4-1.6 N/mm) with average values higher than in the case of jute fibers. This can be explained due to the fact that the jute fibers are characterized by a lower nominal diameter in comparison with curauá and sisal. Consequently, the overall contact area is smaller and hence, the fiber-matrix bond is less influenced by the fiber tortuosity (variation of the cross section along the embedded length and axial twisting) and surface roughness. In the case of sisal fiber these phenomena are also more pronounced since the fiber tortuosity is higher both in terms of cross section area variation (Figure 16b) and axial twisting (Figure 16c) but also because, as highlighted in the previous sections, the sisal fibers present three types of cross section shape.

Finally, also the values reported in Table 3, Table 4 and Table 5 highlight that, for the same embedded length, the sisal fibers exhibit the highest values in terms of G_F: this confirms the above conclusion being attributable to the intrinsic morphology of sisal fibers generally featuring higher surface roughness and more irregular cross section shape than the other natural fibers considered in this study.

5 CONCLUSIONS

This paper is intended as a contribution towards better understanding the interaction between natural fibers and cement-based matrices, which is the main feature controlling the mechanical behavior of natural fiber-reinforced cementitious composites (N-FRCC). The following main points can be remarked:

- the results of the geometric and mechanical characterization of three types of fibers, obtained from different plants, are outlined, along with the results of a series of pull-out tests intended at reproducing either tensile failure in the fiber or bond failure throughout the fiber-to-matrix interface. These results highlighted that the geometric and mechanical properties controlling the behavior of these fibers are somehow comparable to other kinds of “industrial” fibers already employed as spread reinforcement in FRCCs;
- an inverse identification procedure, based on a simplified bilinear bond-slip law (assumed invariant throughout the embedded length of the fiber), has been applied to the force-slip results obtained from pull-out tests in which no tensile rupture was observed: the procedure demonstrated its capability in identifying the bond interaction be-tween fibers and matrix;
- the results obtained from the inverse identification procedure provide relevant insights into the potential of using natural fibers in FRCC. In fact, they highlight the superior performance of sisal fibers (i.e. in terms of resulting

G_F), which emerge as the most suitable to be incorporated as discrete reinforcement in cementitious composites. Furthermore, curauá fibers follow with their slightly lower value of G_F, whereas jute fibers exhibit a G_F in the order of two/three times lower than the sisal ones.

Finally, this study further confirms the preliminary experimental results recently published in the literature for demonstrating feasibility and potential of N-FRCC. Moreover, it provides readers with a structural engineer's vision of their behavior, as it proposes a general identification procedure and reports reference values for the key mechanical parameters needed for predicting the structural response of members made of N-FRCC.

ACKNOWLEDGEMENTS

The present study is part of the activities carried out by the Authors within the "SUPERCONCRETE" Project (www.superconcrete-h2020.unisa.it) funded by the European Union as part of Horizon 2020 (H2020-MSCA-RISE-2014 n°645704).

REFERENCES

[1]. Hannawi K, Bian H, Prince-Agbodjan W, Raghavan B. Effect of different types of fibers on the microstructure and the mechanical behavior of ultra-high performance fiber-reinforced concretes. Composites Part B: Engineering 2016; 86:214-220.

[2]. Gesoglu M, Güneyisi E, Muhyaddin GF, Asaad DS. Strain hardening ultra-high performance fiber reinforced cementitious composites: Effect of fiber type and concentration. Composites Part B: Engineering 2016; 103:74-83.

[3]. Kim SW, Park WS, Jang YI, Feo L, Yun HD. Crack damage mitigation and shear behavior of shear-dominant reinforced concrete beams repaired with strain-hardening cement-based composite. Composites Part B: Engineering 2015; 79:6-19.

[4]. Li VC, Obla K. Effect of fiber diameter variation on properties of cement-based matrix fiber reinforced composites. Composites Part B: Engineering 1996; 27(3-4):275-284.

[5]. Yoo DY, Kim S, Park GJ, Park JJ, Kim SW. Effects of fiber shape, aspect ratio, and volume fraction on flexural behavior of ultra-high-performance fiber-reinforced cement composites. Composite Structures 2017; 174:375-388.

[6]. Lee JH. Influence of concrete strength combined with fiber content in the residual flexural strengths of fiber reinforced concrete. Composite Structures 2017; 168:216-225.

[7]. Simões T, Octávio C, Valença J, Costa H, Dias-da-Costa D, Júlio E. Influence of concrete strength and steel fibre geometry on the fibre/matrix interface. Composites Part B: Engineering 2017; 122:156-164.

[8]. Yan L, Kasal B, Huang L. A review of recent research on the use of cellulosic fibres, their fibre fabric reinforced cementitious, geo-polymer and polymer composites in civil engineering. Composites Part B: Engineering 2016; 92:94-132.

[9]. Codispoti R, Oliveira DV, Olivito RS, Lourenço PB, Fangueiro R. Mechanical performance of natural fiber-reinforced composites for the strengthening of masonry. Composites Part B: Engineering 2015, 77: 74-83.

[10]. Alkbir MFM, Sapuan SM, Nuraini AA, & Ishak MR. Fibre properties and crashworthiness parameters of natural fibre-reinforced composite structure: A literature review. Composite Structures 2016; 148: 59-73.

[11]. Xie X, Zhou Z, Jiang M, Xu X, Wang Z, Hui D. Cellulosic fibers from rice straw and bamboo used as reinforcement of cement-based composites for remarkably improving mechanical properties. Composites Part B: Engineering 2015; 78: 153-161.

[12]. Onuaguluchi O, Banthia N. Plant-based natural fibre reinforced cement composites: A review. Cement and Concrete Composites 2016; 68:96-108.

[13]. Lau KT, Hung PY, Zhu MH, Hui D. Properties of natural fibre composites for structural engineering applications. Composites Part B: Engineering 2018; 136: 222-233.

[14]. Barros JA, Ferrara L, Martinelli E (Eds.). Recent Advances on Green Concrete for Structural Purposes: The contribution of the EU-FP7 Project EnCoRe. Springer, 2017.

[15]. Pacheco-Torgal F, Jalali S. Cementitious building materials reinforced with vegetable fibres: A review. Construction and Building Materials 2011; 25(2):575-581.

[16]. Ramzy A, Beermann D, Steuernagel L, Meiners D, Ziegmann G. Developing a new generation of sisal composite fibres for use in industrial applications. Composites Part B: Engineering 2014; 66:287-298.

[17]. Węcławski BT, Fan M, Hui D. Compressive behaviour of natural fibre composite. Composites Part B: Engineering 2014; 67:183-191.

[18]. Sepe R, Bollino F, Boccarusso L, Caputo F. Influence of chemical treatments on mechanical properties of hemp fiber reinforced composites. Composites Part B: Engineering 2018; 133: 210-221.

[19]. Živković I, Fragassa C, Pavlović A, Brugo T. Influence of moisture absorption on the impact properties of flax, basalt and hybrid flax/basalt fiber reinforced green composites. Composites Part B: Engineering 2017, 111:148-164.

[20]. Pickering KL, Efendy MA, Le TM. A review of recent developments in natural fibre composites and their mechanical performance. Composites Part A: Applied Science and Manufacturing 2016; 83:98-112.

[21]. Ardanuy M, Claramunt J, Toledo Filho RD. Cellulosic fiber reinforced cement-based composites: a review of recent research. Construction and Building Materials 2015; 79:115-128.

[22]. Ferreira SR, de Andrade Silva F, Lima PRL, Toledo Filho RD. Effect of hornification on the structure, tensile behavior and fiber matrix bond of sisal, jute and curauá fiber cement based composite systems. Construction and Building Materials 2017; 139:551-561.

[23]. Zhou Y, Fan M, Chen L. Interface and bonding mechanisms of plant fibre composites: An overview. Composites Part B: Engineering 2016; 101:31-45.

[24]. Li Y, Bielak J, Hegger J, Chudoba R. An incremental inverse analysis procedure for identification of bond-slip laws in composites applied to textile reinforced concrete. Composites Part B: Engineering 2018; 137:111-122.

[25]. Ferreira SR, Martinelli E, Pepe M, de Andrade Silva F, Toledo Filho RD. Inverse identification of the bond behavior for jute fibers in cementitious matrix. Composites Part B: Engineering 2016; 95:440-452.

[26]. Silva FA, Chawla N, Toledo Filho RD. An experimental investigation of the fatigue behavior of sisal fibers. Materials Science and Engineering: A 2009; 516(1):90-95.

[27]. NBR 11578: 1991. Portland composite cement – Specification. ABNT - Associação Brasileira de Normas Técnicas.

[28]. Ferreira SR, Lima, PRL, Silva FA, Toledo Filho RD. Effect of sisal fiber hornification on the fiber-matrix bonding characteristics and bending behavior of cement based composites. Key Engineering Materials 2014; 600:421-432.

[29]. https://imagej.nih.gov/ij/ ImageJ: Image Processing and Analysis in Java. Accessed on April 2017.

[30]. ASTM C1557-14. Standard Test Method for Tensile Strength and Young's Modulus of Fibers, ASTM International, West Conshohocken, PA, 2014.

[31]. ASTM C642-13. Standard Test Method for Density, Absorption, and Voids in Hardened Concrete, ASTM International, West Conshohocken, PA, 2013.

[32]. ASTM C1437-15. Standard Test Method for Flow of Hydraulic Cement Mortar, ASTM International, West Conshohocken, PA, 2015.

[33]. ASTM C39/C39M-15a. Standard Test Method for Compressive Strength of Cylindrical Concrete Specimens, ASTM International, West Conshohocken, PA, 2015.

[34]. ASTM C469/C469M-14. Standard Test Method for Static Modulus of Elasticity and Poisson's Ratio of Concrete in Compression, ASTM International, West Conshohocken, PA, 2014.

[35]. RILEM Technical Committee 232-TDT: Test methods and design of textile reinforced concrete.

[36]. Silva FDA, Mobasher B, Soranakom C, Toledo Filho RD. Effect of fiber shape and morphology on interfacial bond and cracking behaviors of sisal fiber cement based composites. Cement and Concrete Composites 2011; 33(8):814-823.

[37]. Silva FDA, Toledo Filho RD, Mobasher B, Chawla N. A multi-scale investigation of the mechanical behavior of durable sisal fiber cement compo-sites. Matéria (Rio de Janeiro) 2010; 15(2):338-344.

[38]. Naaman AE. Fibers with Slip-Hardening Bond. In: PRO 6: 3rd International RILEM Workshop on High Performance Fiber Reinforced Cement Composites (HPFRCC 3) 1999; 3:371. RILEM Publications.

[39]. Naaman AE. Engineered steel fibers with optimal properties for reinforcement of cement composites. Journal of advanced concrete technology 2003; 1(3):241-252.

[40]. Fidelis MEA, Pereira TVC, Gomes OFM, Silva FA, Toledo Filho RD. The effect of fiber morphology on the tensile strength of natural fibers. Journal of Materials Research and Technology 2013; 2(2):149-157.

[41]. Caggiano A, Martinelli E, Faella C. A fully-analytical approach for modelling the response of FRP plates bonded to a brittle substrate. International Journal of Solids and Structures 2012; 49(17): 2291-2300.

[42]. Silva FA, D, Chawla N Toledo Filho R. Tensile behavior of high performance natural (sisal) fibers. Composites Science Technology 2008; 68(15):3438-3443

[43]. Fimberl P, B. Siffert B. Interaction of calcium carbonate (calcite) with cellulose fibres in aqueous medium. Colloids and surfaces 1986, 20:1- 16.

[44]. Torre M, Rodrigue AR, Calixto FS. Study of the interactions of calcium ions with lignin, cellulose and pectin. Journal of Agricultural and Food Chemistry 1992; 40: 1762-1766.

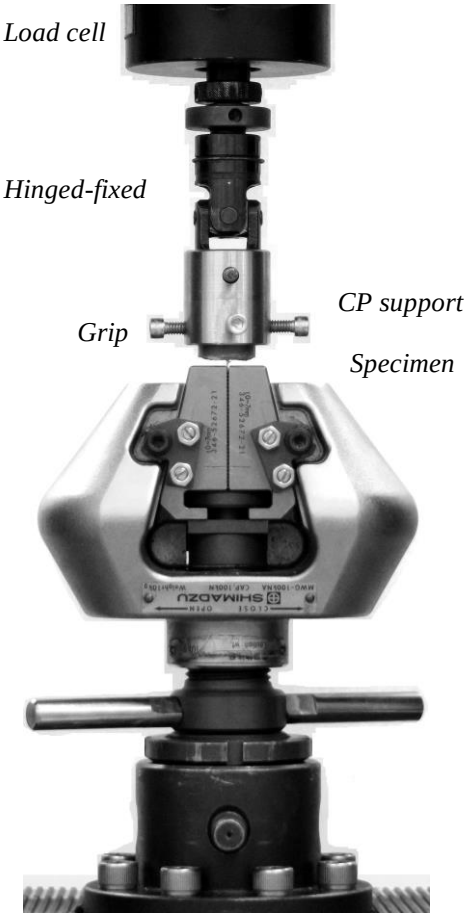

Figure 1: Pullout test setup.

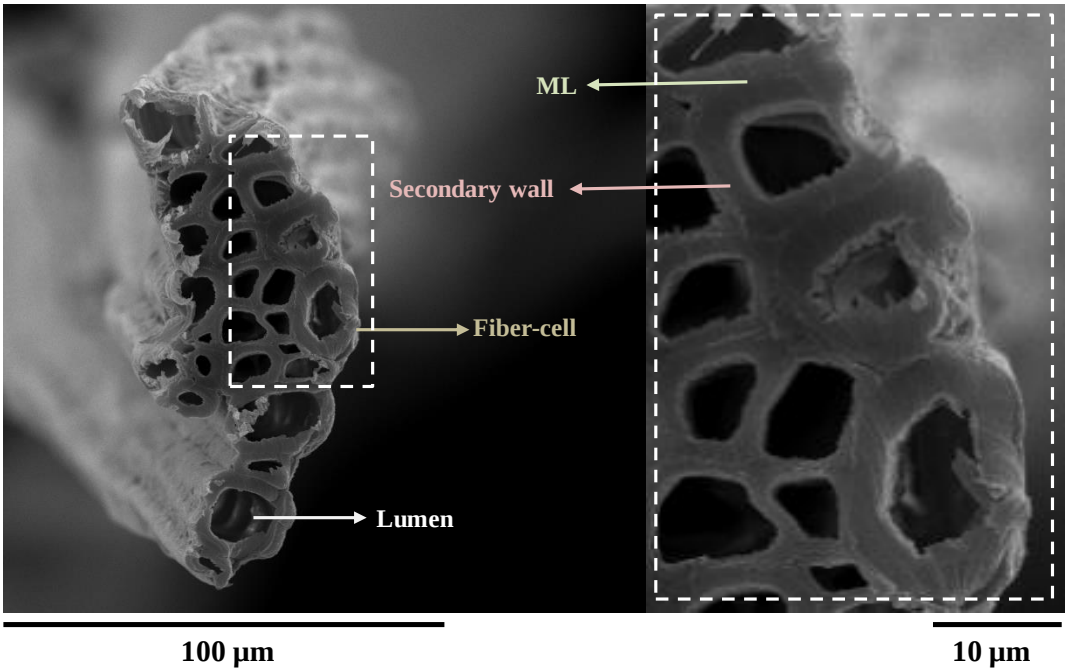

Figure 2: Typical microstructure of a natural fiber.

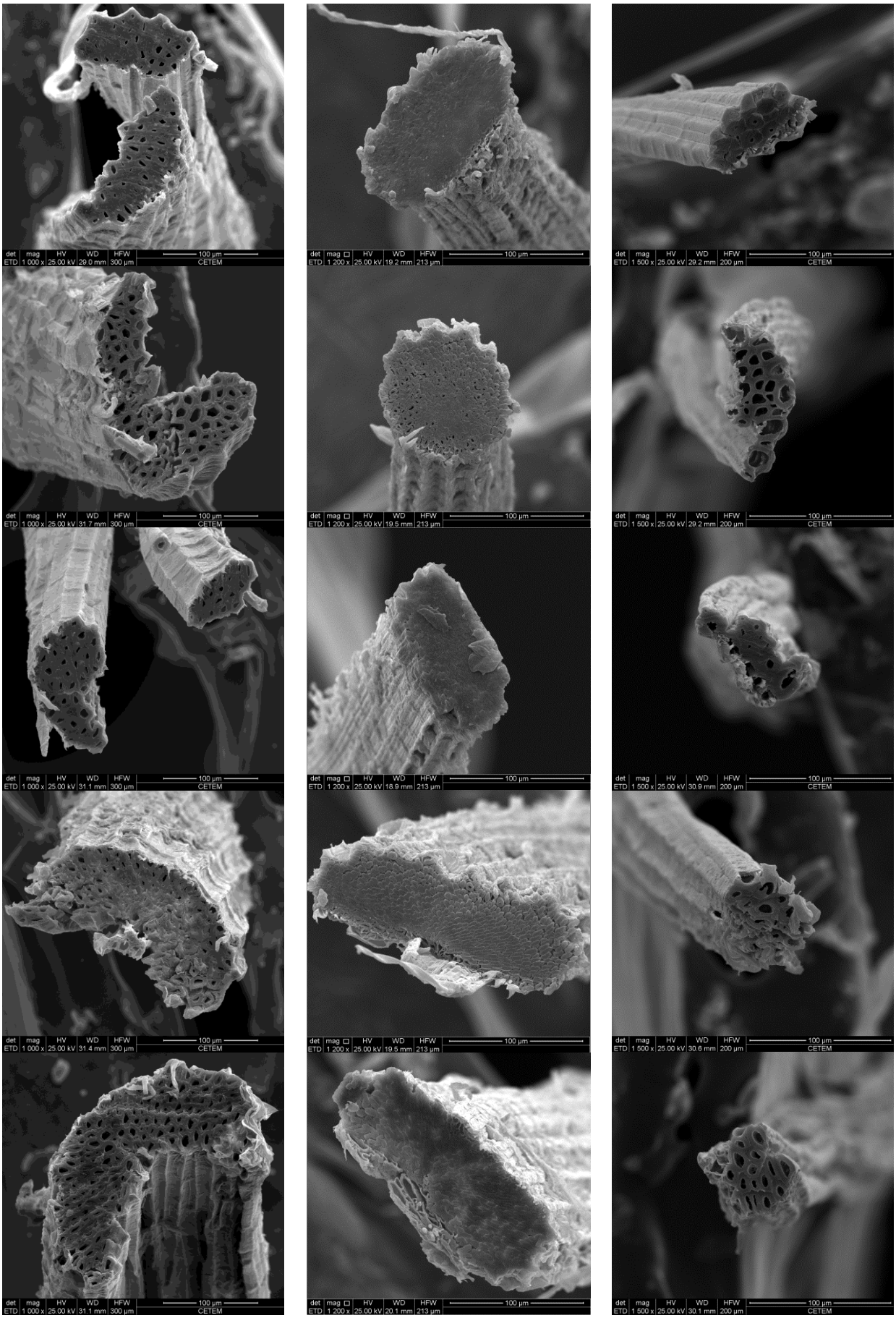

(a) Sisal *(b) Curauá* *(c) Jute*

Figure 3: Examples of cross sections: (a) sisal, (b) curauá and (c) jute fibers.

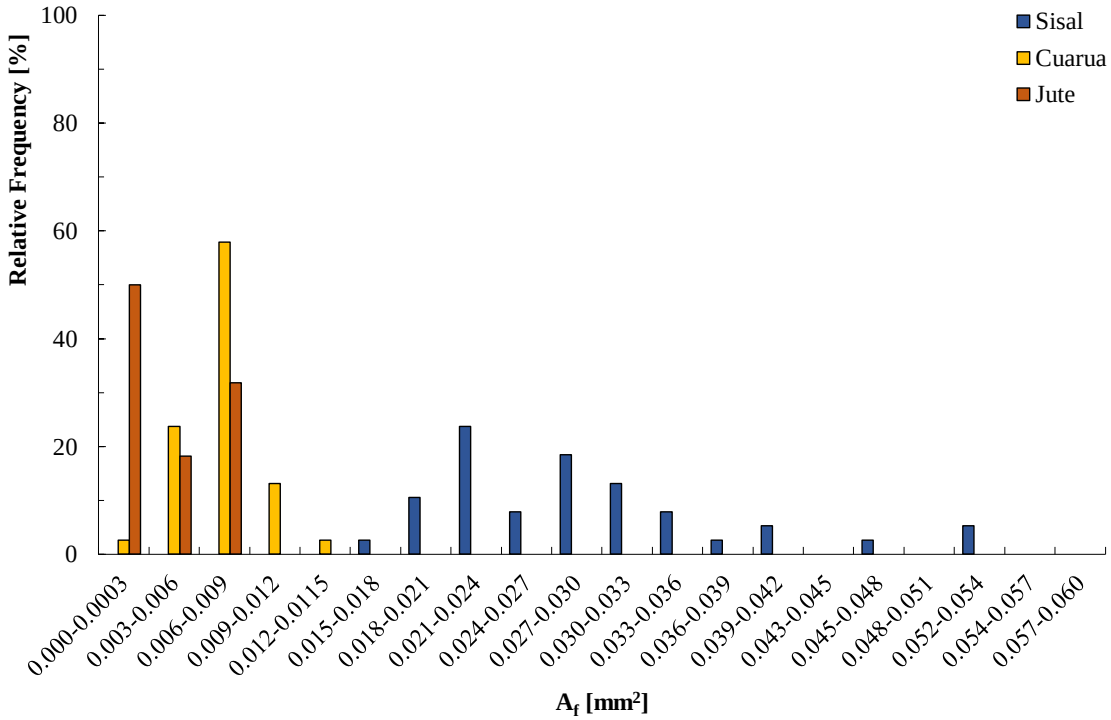

Figure 4: Relative frequency distribution for cross-section area of natural fibers.

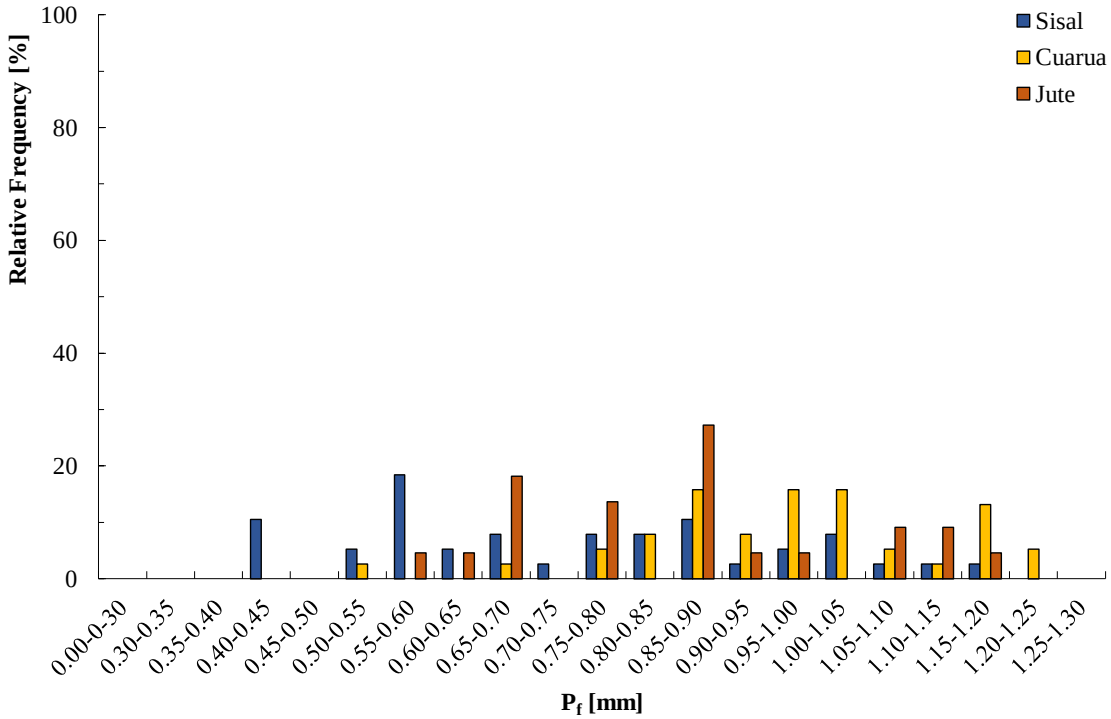

Figure 5: Relative frequency distribution for perimeter of natural fibers.

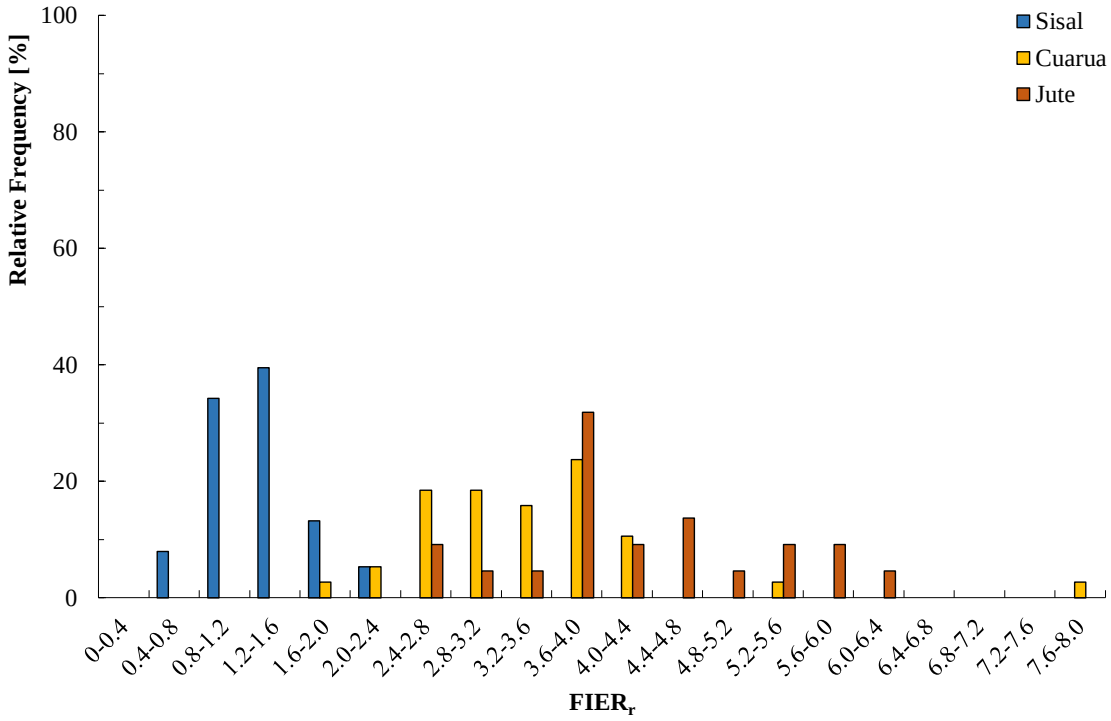

Figure 6: Relative frequency distribution for relative FIER of natural fibers.

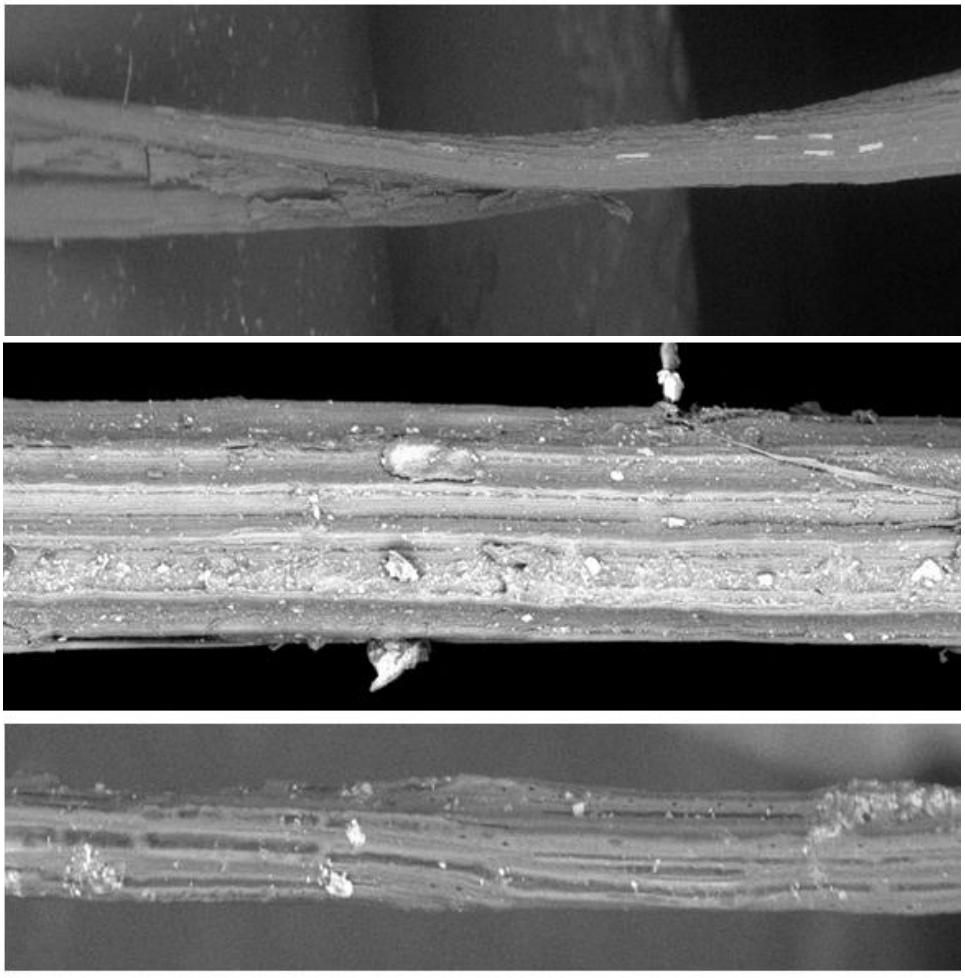

Figure 7: A comparison between sisal, curauá and jute fiber rotation in its axis.

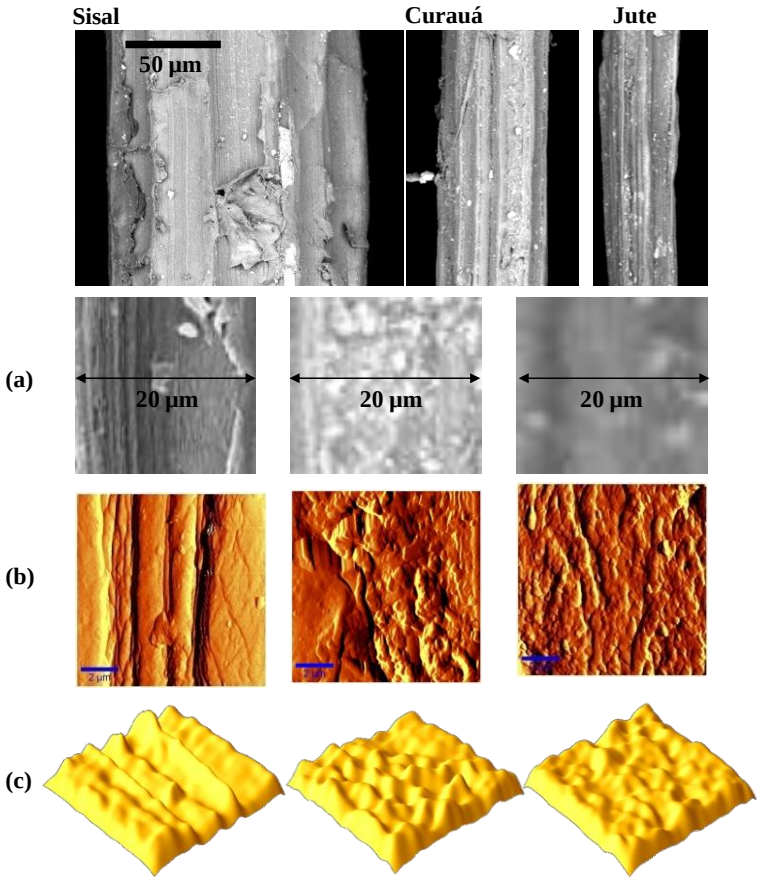

Figure 8: Surface morphology of the natural fibers: sisal, curauá and jute respectively: (a) SEM microscopy, (b) AFM phase contrast images (20 µm x 20 µm) and (c). 3D view by imageJ from AFM images and roughness values obtained from 5 different scans.

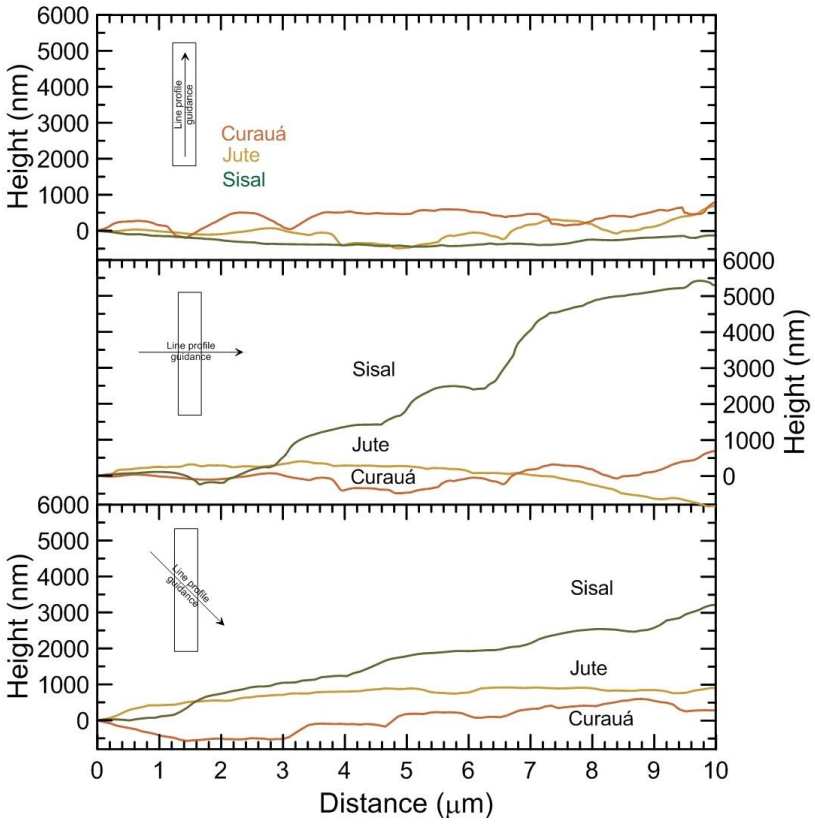

Figure 9: Transversal and longitudinal surface roughness for natural fibers.

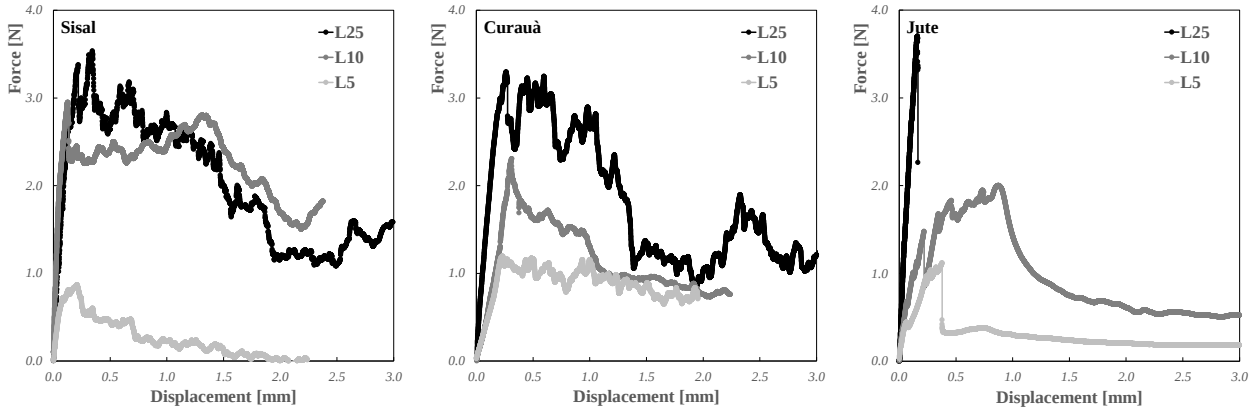

Figure 10: Typical pull-out behavior of natural fibers.

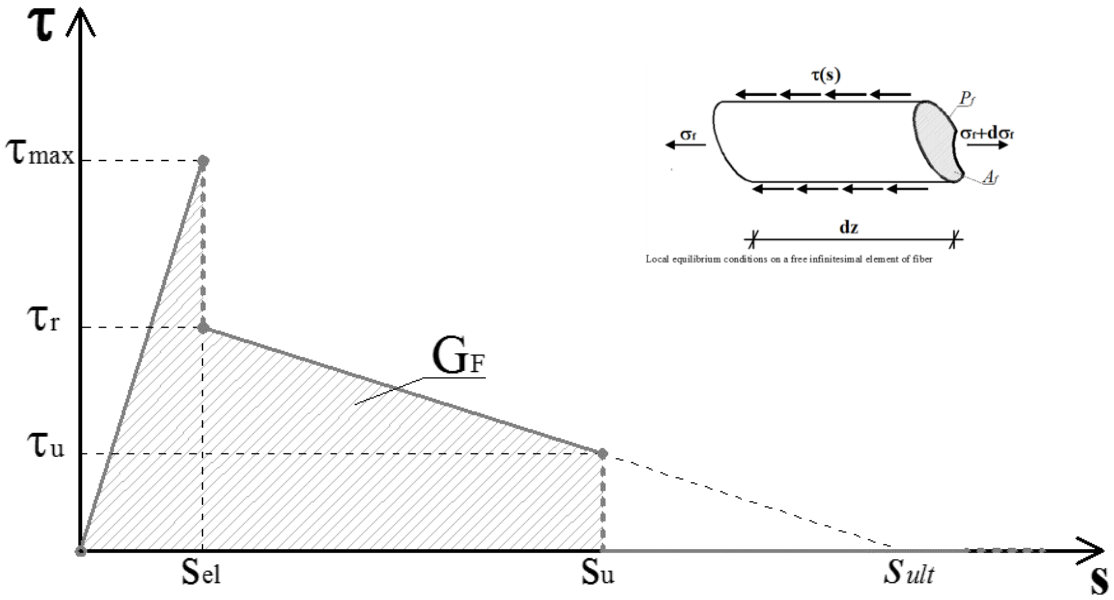

Figure 11. Bilinear bond-slip relationship.

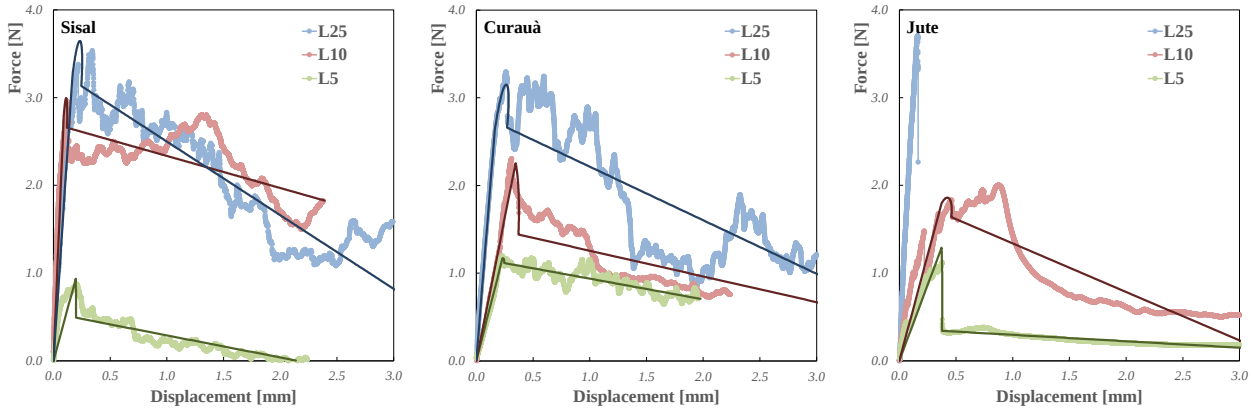

Figure 12: Experimental versus model.

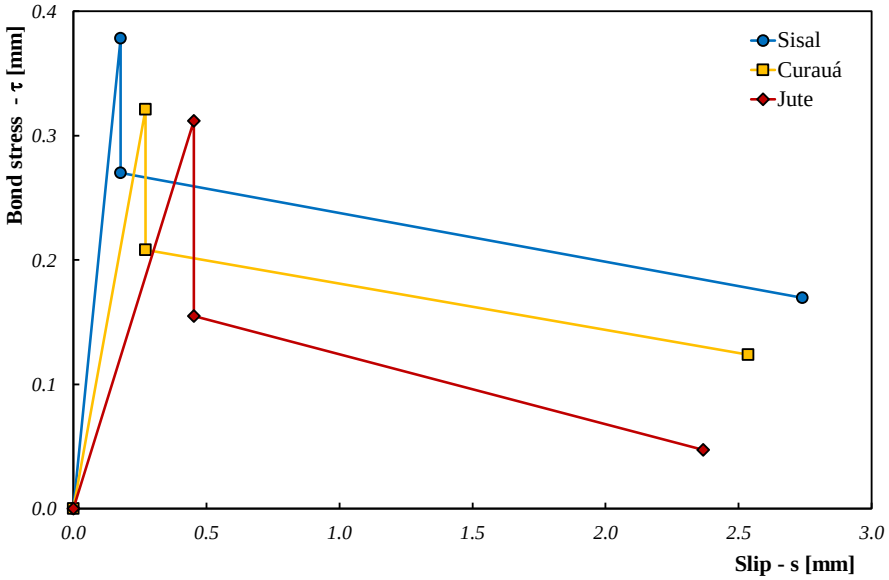

Figure 13: "Average" bond-slip laws for natural fibers.

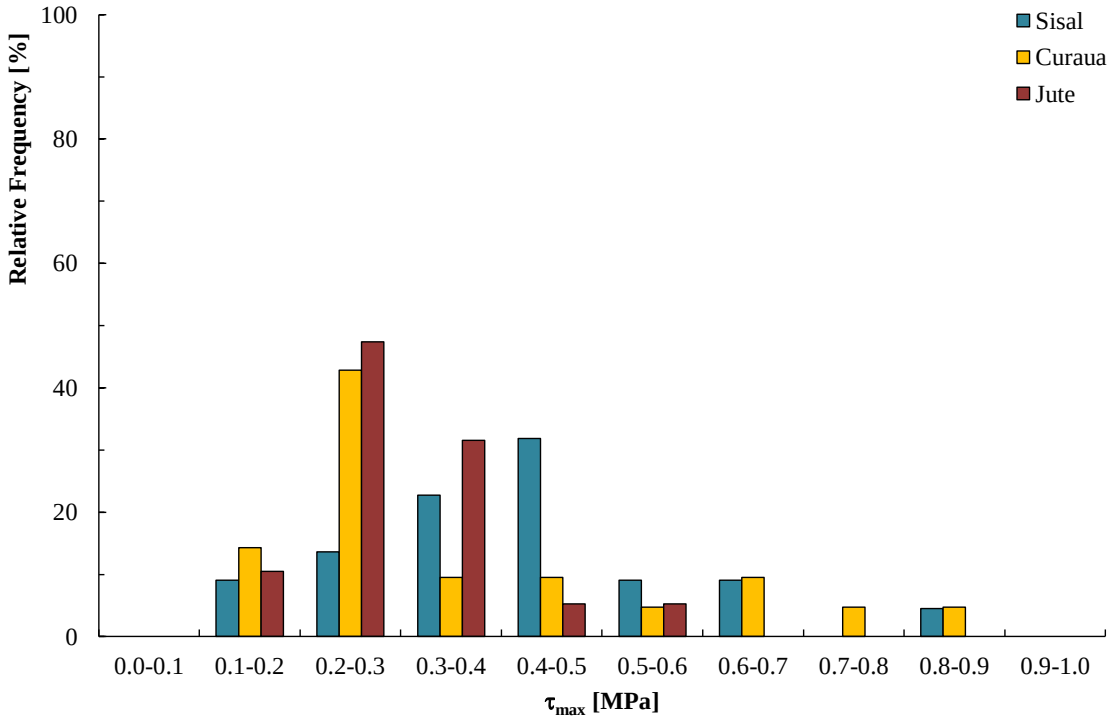

Figure 14: Relative frequency distribution for τ_{max} values.

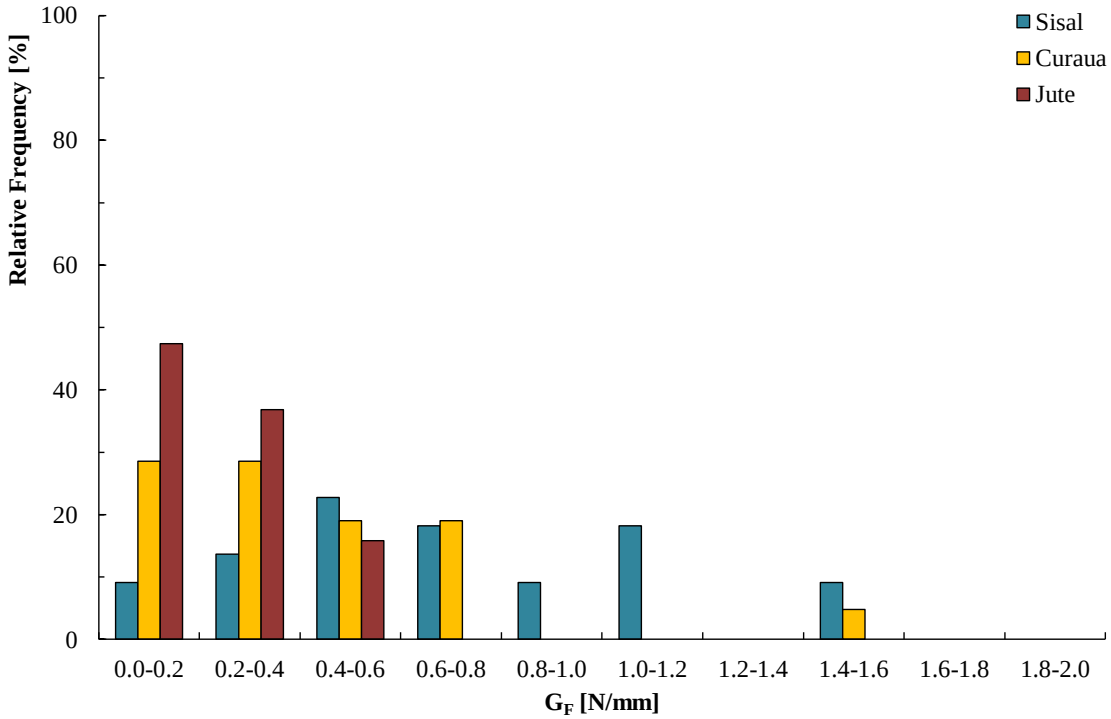

Figure 15: Relative frequency distribution for G_F values.

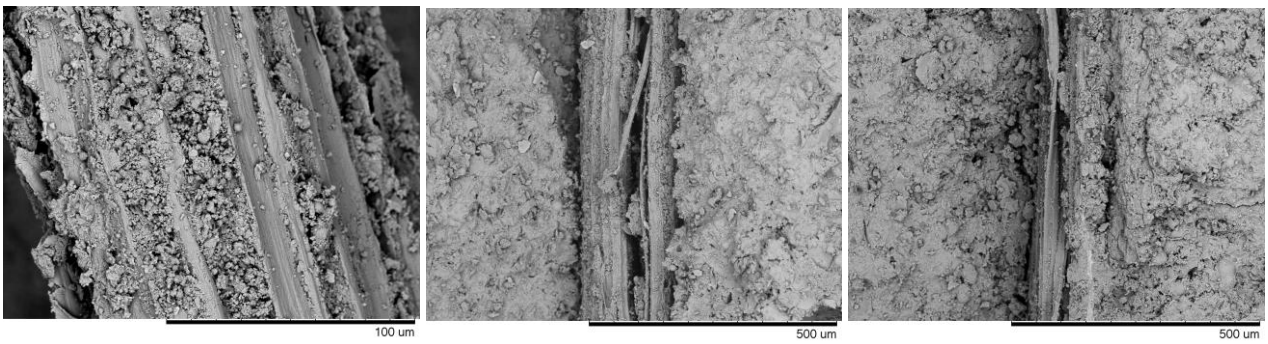

Figure 16: SEM images of sisal fibers after pull-out test: (a) hydration products on sisal fiber surface; (b) (c) fiber embedded in cement based matrix.

Table 1: Physical and mechanical characterization of the cement matrix

Properties		***Value (cv)***
Absorption	A	4.97 % (0.10%)
Density	ρ	2.16 g/cm^3 (0.22%)
Void content		9.16 (0.54%)
Flow table spread value		450 mm
Compressive strength at 7 days	$f_{c,7}$	22.00 MPa
Compressive strength at 28 days	$f_{c,28}$	33.56 MPa (4.39%)
Elastic Modulus	E	13.27 GPa (2.34%)
Tensile strength	f_t	2.24 MPa (12.31%)

Table 2: Measurement results for area and diameter of lumens, number and thickness of cell wall for sisal, curauá, and jute.

Fibers	***Number of fiber-cells***	***Lumens area [µm²]***	***Diameter of lumens [µm]***	***Microfibrils angle orientation***	***Real area [mm²]***	***Total area [mm²]***
Sisal	144	5796.9	8.2	10-22	0.017	0.023
Curauá	300	358.93	0.8	18	0.007	0.008
Jute	26	1014.1	6.7	17	0.003	0.004

Table 3: Bond-slip law for the sisal fibers.

l_b [mm]	#	s_e [mm]	s_u [mm]	τ_{max} [MPa]	τ_r [MPa]	τ_u [MPa]	G_F [N/mm]
5	1	0.250	3.131	0.549	0.520	0.223	1.139
	2	0.196	2.150	0.325	0.169	0.000	0.197
	3	0.345	3.313	0.334	0.208	0.089	0.497
	4	0.112	3.128	0.608	0.326	0.322	1.011
	5	0.178	4.006	0.280	0.243	0.081	0.646
	6	0.184	3.092	0.335	0.237	0.235	0.718
	7	0.132	2.105	0.191	0.126	0.062	0.198
	8	0.138	3.507	0.333	0.314	0.311	1.076
	9	0.132	2.100	0.275	0.211	0.198	0.420
	10	0.190	3.306	0.436	0.423	0.256	1.100
	11	0.097	3.787	0.604	0.379	0.372	1.414
	average (cov)	***0.18 (38)***	***3.06 (21)***	***0.39 (35)***	***0.29 (39)***	***0.20 (59)***	***0.77 (51)***
10	1	0.205	3.081	0.434	0.431	0.189	0.936
	2	0.211	2.269	0.892	0.292	0.049	0.445
	3	0.338	3.277	0.312	0.185	0.086	0.451
	4	0.155	3.067	0.420	0.256	0.254	0.775
	5	0.290	3.842	0.552	0.534	0.317	1.591
	6	0.116	3.215	0.118	0.109	0.080	0.300
	7	0.090	2.400	0.422	0.318	0.217	0.637
	8	0.089	1.199	0.468	0.364	0.213	0.341
	9	0.248	2.069	0.207	0.198	0.156	0.349
	10	0.224	2.051	0.477	0.477	0.379	0.836
	11	0.146	1.273	0.452	0.418	0.294	0.434
	average (cov)	***0.19 (40)***	***2.52 (32)***	***0.43 (44)***	***0.33 (39)***	***0.20 (49)***	***0.64 (56)***
25	1	0.233	3.087	0.199	0.173	0.075	0.378
	2	0.160	2.148	0.295	0.121	0.000	0.144
	3	0.105	2.847	0.188	0.068	0.061	0.187
	4	0.167	3.025	0.165	0.113	0.028	0.215
	5	0.036	1.503	0.339	0.075	0.035	0.087
	average (cov)	***0.14 (47)***	***2.52 (24)***	***0.24 (28)***	***0.11 (34)***	***0.04 (66)***	***0.20 (48)***

Table 4: Bond-slip law for the curauà fibers.

l_b [mm]	#	s_e [mm]	s_u [mm]	τ_{max} [MPa]	τ_r [MPa]	τ_u [MPa]	G_F [N/mm]
5	1	0.052	1.243	0.202	0.181	0.103	0.174
	2	0.268	2.908	0.251	0.241	0.205	0.622
	3	0.285	0.692	0.891	0.872	0.208	0.347
	4	0.621	1.182	0.160	0.093	0.040	0.087
	5	0.280	2.644	0.211	0.079	0.014	0.138
	6	0.231	1.992	0.206	0.186	0.117	0.291
	7	0.310	2.941	0.639	0.571	0.478	1.479
	8	0.107	1.325	0.198	0.117	0.116	0.152
	9	0.209	1.875	0.268	0.268	0.265	0.472
	10	0.186	2.245	0.714	0.394	0.136	0.613
	11	0.204	0.484	0.373	0.344	0.340	0.134
	average (cov)	***0.25 (55)***	***1.78 (46)***	***0.37 (65)***	***0.30 (75)***	***0.18 (71)***	***0.41 (94)***
10	1	0.306	3.770	0.367	0.221	0.190	0.767
	2	0.319	3.107	0.296	0.182	0.180	0.552
	3	0.150	3.737	0.204	0.136	0.134	0.500
	4	0.516	2.900	0.216	0.135	0.105	0.342
	5	0.203	2.498	0.153	0.073	0.028	0.131
	6	0.313	3.708	0.448	0.259	0.105	0.688
	7	0.150	1.638	0.538	0.184	0.096	0.248
	8	0.656	3.698	0.260	0.083	0.082	0.337
	9	0.150	3.023	0.406	0.179	0.070	0.388
	10	0.172	2.902	0.604	0.268	0.107	0.564
	average (cov)	***0.29 (55)***	***3.10 (20)***	***0.35 (43)***	***0.17 (38)***	***0.11 (41)***	***0.45 (42)***
25	1	0.150	3.024	0.127	0.081	0.072	0.229
	2	0.559	1.861	0.083	0.066	0.049	0.098
	3	0.634	3.062	0.161	0.139	0.115	0.360
	4	0.097	3.019	0.204	0.154	0.146	0.449
	5	0.150	3.302	0.213	0.075	0.062	0.232
	6	0.163	3.336	0.164	0.102	0.030	0.223
	7	0.255	3.684	0.323	0.145	0.000	0.290
	8	0.152	1.750	0.430	0.212	0.001	0.203
	average (cov)	***0.27 (72)***	***2.88 (23)***	***0.21 (49)***	***0.12 (38)***	***0.06 (82)***	***0.26 (38)***

Table 5: Bond-slip law for the jute fibers.

l_b [mm]	#	s_e [mm]	s_u [mm]	τ_{max} [MPa]	τ_r [MPa]	τ_u [MPa]	G_F [N/mm]
5	1	0.373	3.145	0.241	0.063	0.025	0.167
	2	0.653	3.212	0.268	0.056	0.010	0.171
	3	0.217	2.048	0.292	0.099	0.000	0.122
	4	0.825	3.135	0.299	0.138	0.031	0.319
	5	0.546	3.537	0.271	0.215	0.111	0.562
	6	0.489	1.765	0.368	0.098	0.092	0.211
	7	0.562	1.594	0.294	0.133	0.090	0.198
	8	0.365	1.544	0.260	0.145	0.058	0.167
	9	0.448	1.577	0.392	0.167	0.108	0.243
	10	0.466	1.588	0.337	0.084	0.083	0.172
	11	0.201	1.475	0.303	0.188	0.024	0.166
	12	0.218	1.942	0.246	0.114	0.003	0.128
	average (cov)	***0.45 (40)***	***2.21 (34)***	***0.30 (15)***	***0.13 (38)***	***0.05 (76)***	***0.22 (53)***
10	1	0.582	3.258	0.168	0.149	0.020	0.275
	2	0.363	2.913	0.449	0.285	0.001	0.446
	3	0.961	2.030	0.171	0.141	0.047	0.183
	4	0.345	2.342	0.361	0.163	0.055	0.280
	5	0.245	3.010	0.376	0.250	0.046	0.455
	6	0.356	1.731	0.547	0.238	0.071	0.310
	7	0.373	3.116	0.283	0.219	0.022	0.383
	average (cov)	***0.46 (49)***	***2.63 (21)***	***0.34 (39)***	***0.21 (25)***	***0.04 (59)***	***0.33 (28)***

The final version of this manuscript is available in *Composites Part B: Engineering*. 10.1016/j.compositesb.2017.12.016